THE JOURNAL OF BIOLOGICAL CHEMISTRY VOL. 288, NO. 15, pp. 10459–10471, April 12, 2013

The REV7 Subunit of DNA Polymerase ζ Is Essential for Primordial Germ Cell Maintenance in the Mouse*

Received for publication, September 22, 2012, and in revised form, March 5, 2013 Published, JBC Papers in Press, March 5, 2013, DOI 10.1074/jbc.M112.421966

Naoki Watanabe[‡1], Shinji Mii[‡1], Naoya Asai[§], Masato Asai[‡], Kaoru Niimi[‡¶], Kaori Ushida[‡], Takuya Kato[‡], Atsushi Enomoto[‡], Hideshi Ishii[‖], Masahide Takahashi[‡§], and Yoshiki Murakumo[‡2]**

From the Departments of [‡]Pathology and [¶]Obstetrics and Gynecology and the [§]Division of Molecular Pathology, Center for Neurological Disease and Cancer, Nagoya University Graduate School of Medicine, 65 Tsurumai-cho, Showa-ku, Nagoya 466-8550, the [‖]Department of Gastroenterological Surgery, Osaka University Graduate School of Medicine, 2-2 Yamadaoka, Suita, Osaka 565-0871, and the [**]Department of Pathology, Kitasato University School of Medicine, 1-15-1 Kitasato, Minami-ku, Sagamihara, Kanagawa 252-0374, Japan

Background: Biological significance of REV7 in mouse development has not been elucidated.
Results: REV7-deficient mice show germ cell aplasia at birth in both sexes, and primordial germ cells (PGCs) were lost because of apoptosis during migration at an early embryonic stage.
Conclusion: REV7 is essential for PGC maintenance in the mouse.
Significance: REV7 is a novel regulator of PGC survival.

REV7 (also known as MAD2L2 and MAD2B) is involved in DNA repair, cell cycle regulation, gene expression, and carcinogenesis. *In vitro* studies show that REV7 interacts with several proteins and regulates their function. It has been reported that human *REV7* is highly expressed in the adult testis by Northern blot analysis. However, the significance of REV7 in mammalian development has not been elucidated. Here, we present analyses of REV7-deficient (*Rev7*$^{-/-}$) mice to clarify the significance of *Rev7* in mouse development. In WT mice (*Rev7*$^{+/+}$), *Rev7* expression was ubiquitously observed in the embryo and confined to germ cells in the testes after birth. *Rev7*$^{-/-}$ mice exhibited growth retardation and a partial embryonic lethal phenotype. Mice that survived to adulthood were infertile in both sexes and showed germ cell aplasia in the testes and ovaries. Analyses of *Rev7*$^{-/-}$ embryos revealed that primordial germ cells (PGCs) were present at embryonic day 8.5 (E8.5). However, progressive loss of PGCs was observed during migration, and PGCs were absent in the genital ridges at E13.5. An increase of apoptotic cells was detected not only among PGCs but also in the forebrain of the *Rev7*$^{-/-}$ embryo, whereas cell proliferation was unaffected. Moreover, DNA damage accumulation and increased levels of histone methylation were detected in *Rev7*$^{-/-}$ embryos, and expression of *Oct4* and *Nanog* was deregulated by REV7 deficiency at E8.5. These findings indicate that *Rev7* is essential for PGC maintenance by prevention of apoptotic cell death in the mouse.

Germ cell development in mice is regulated by specific genetic and epigenetic factors. Germ cells arise from pluripotent epiblast cells and are characterized as alkaline phosphatase-positive primordial germ cells (PGCs)[3] that form a cluster of about 40–45 cells inside the extra-embryonic mesoderm at the posterior end of the primitive streak at around embryonic day 7.25 (E7.25). Subsequently, they migrate through the hindgut endoderm and reach the genital ridges by E11.5, where they proliferate and differentiate to spermatozoa or oocytes from E13.0 (1–4). By the time of sexual differentiation, the number of PGCs increases to ~25,000. Before germ cell specification, bone morphogenetic protein 4 (BMP4), BMP8b, and BMP2 secreted from the extraembryonic ectoderm and visceral endoderm induce the formation of PGC precursor cells in the proximal epiblast. These PGC precursor cells express transcriptional regulators B lymphocyte maturation-induced protein 1 (Blimp1) and PR domain containing 14 (Prdm14). The former suppresses gene expression required for somatic cell differentiation, such as *Snail* and *Hox* genes, and the latter controls genome-wide epigenetic reprogramming in PGCs (2, 5–7). During PGC migration, expression of Nanos3 and c-Kit is essential for PGC maintenance. Nanos3 is an RNA-binding protein expressed in PGCs after E7.5 and prevents apoptosis of PGCs during migration (8). c-Kit is a receptor tyrosine kinase, and the signal from the c-Kit ligand is required for proliferation and directed migration of PGCs (9). In addition, some knockout mouse studies have revealed essential factors for PGC survival between E8.5 and E13.5, including RNA-binding protein dead end 1 (Dnd1), T cell-restricted intracellular antigen 1-related protein (TIAR), a homeodomain transcription factor of the POU family, Oct4, and a unique homeoprotein transcription factor, Nanog (10–13). Epigenetic modification also

* This work was supported by Grants-in-aid for Global Center of Excellence (GCOE) Research and for Scientific Research (A) commissioned by the Ministry of Education, Culture, Sports, Science and Technology (MEXT) of Japan (to M. T.), and by Grants-in-aid for Scientific Research (C) commissioned by MEXT of Japan (to Y. M.).
[1] Both authors contributed equally to this work.
[2] To whom correspondence should be addressed: Dept. of Pathology, Kitasato University School of Medicine, 1-15-1 Kitasato, Minami-ku, Sagamihara, Kanagawa 252-0374, Japan. Tel.: 81-42-778-9020; Fax: 81-42-778-9124; E-mail: murakumo@med.kitasato-u.ac.jp.

[3] The abbreviations used are: PGC, primordial germ cell; TIAR, T cell-restricted intracellular antigen 1-related protein; Pol, polymerase; PLZF, promyelocytic leukemia zinc finger protein; PCNA, proliferating cell nuclear antigen; DAB, diaminobenzidine; DIG, digoxigenin; E, embryonic day; P, postnatal day.

occurs during PGC migration. Reduction of H3K9 dimethylation (H3K9me2) and up-regulation of H3K27 trimethylation (H3K27me3) are principal epigenetic modifications after E8.5, which control the chromatin state of the PGC genome (14, 15). PGCs proliferate for another 1 or 2 days after they colonize the genital ridges and then differentiate into spermatozoa or oocytes (16).

REV7 (also named MAD2L2 and MAD2B) is a protein involved in DNA repair, cell cycle regulation, gene expression, and carcinogenesis. In the yeast *Saccharomyces cerevisiae*, Rev7 and Rev3 bind to each other to form DNA polymerase ζ (Pol ζ), in which Rev3 is a catalytic subunit possessing a polymerase activity and Rev7 is an accessory subunit (17). Pol ζ is a member of the specialized low fidelity DNA polymerases, including Y-family polymerases, Pol η, Pol ι, Pol κ, and Rev1, which are capable of synthesizing DNA at DNA lesions via a mechanism called translesion DNA synthesis (18). Rev7 enhances the polymerase activity of Rev3, indicating the involvement of Rev7 in the DNA damage response (17). A human homolog of yeast Rev7 has been identified as an interacting partner of human REV3 (19). REV7 also interacts with human REV1, but the biological significance of REV7 association with REV3 and REV1 in humans is unclear (20–22). Human fibroblasts with siRNA-mediated depletion of *REV7* expression show high sensitivity to UV-induced cytotoxicity and reduced sensitivity to UV-induced mutagenesis compared with those in control lines, indicating that REV7 is required for tolerance to UV-induced DNA damage (23). Recently, it has been reported that Pol ζ and REV1 are involved in homologous recombination repair of DNA double strand breaks, although its mechanism is not fully understood (24, 25).

On the other hand, REV7 has been identified as the second human homolog of *S. cerevisiae* Mad2 (26). REV7 binds to CDH1 and CDC20, which are cell cycle regulating proteins, and inhibits the anaphase-promoting complex that degrades cyclin B1 (27, 28). When recombinant human REV7 protein was injected into *Xenopus* embryos, gastrulation was dramatically arrested (28). REV7 also interacts with the *Shigella* effector IpaB, and mediates cell cycle arrest of *Shigella*-infected epithelial cells (29). IpaB-bound REV7 is sequestered away from CDH1, causing unscheduled activation of the anaphase-promoting complex, which disrupts cell cycle-dependent regulation of cyclin B1 expression, resulting in cell cycle arrest at the G_2/M phase in *Shigella*-infected epithelial cells. These findings indicate that REV7 is involved in cell cycle regulation. In addition, it has been reported that REV7 interacts with the transcription factor ELK-1 and regulates expression of its target genes, *egr-1* and c-*fos*, after treatment with DNA-damaging agents (30). REV7 also interacts with TCF-4, a component of the WNT signaling pathway, and modulates TCF-4-mediated E-cadherin expression (31). Moreover, it has been reported that several proteins involved in carcinogenesis, such as PRCC (papillary renal cell carcinoma) and HCCA2 (hepatocellular carcinoma-associated gene 2), interact with REV7. Increased levels of *REV7* mRNA in colon cancer are significantly correlated with reduced patient survival, suggesting that REV7 is associated with human cancer biology (32–34). However, the significance of REV7 in mammalian development has not yet been elucidated.

In the present study, we generated REV7-deficient ($Rev7^{-/-}$) mice and analyzed their phenotypes to understand the biological significance of REV7 in mouse development. We show that REV7 is involved in the prevention of apoptotic cell death of PGCs and is essential for PGC maintenance in the embryo. Our findings indicate the importance of REV7 expression in mouse development.

EXPERIMENTAL PROCEDURES

Vector Construction—The targeting vector was constructed using pBlueScript II KS (Agilent Technologies) possessing a neomycin (*neo*) selection marker with a phosphoglycerate kinase (*PGK*) promoter. A 1330-bp genomic fragment upstream of the start codon of the mouse *Rev7* locus was synthesized by PCR and inserted before the *PGK-neo* cassette. A 5110-bp genomic sequence (containing *Rev7* exon 3–8) was synthesized by PCR and inserted after the *PGK-neo* cassette (Fig. 1*A*). PCR products were generated using PfuUltra™ High Fidelity DNA polymerase (Agilent Technologies), and genomic DNA from the 129SvJ strain was used as a template. The targeting vector was verified by DNA sequencing and restriction mapping.

Generation of Rev7-Knock-out Mice—The targeting vector was linearized and introduced by electroporation into ES cells derived from 129SvJ mice. After G418/diphtheria toxin A positive-negative selection, two ES cell clones with successful homologous recombination were identified by Southern blot screening of NheI-digested genomic DNA with a 5′ probe (Fig. 1*A*). The two clones were injected into C57BL/6J blastocysts and chimeric mice were generated by PhoenixBio. The genetic background of the mice used in this study was C57BL6J/129SvJ. All mice were housed in polycarbonate cages containing hardwood chip bedding at 25 °C with a 12-h light/dark cycle. All animal protocols were approved by the Animal Care and Use Committee of Nagoya University Graduate School of Medicine.

Mouse Genotyping—Genomic DNAs extracted from mouse tail biopsies were used for PCR genotyping. Sequences of the primer sets used for genotyping are listed in Table 1. PCR products of WT and targeted alleles were 230 and 750 bp, respectively. Templates were amplified with ExTaq polymerase (Takara).

Southern Blot Screening—Mouse genomic DNAs were digested with NheI. The 5′ probe indicated in Fig. 1*A* was radiolabeled with [^{32}P]dCTP (PerkinElmer Life Sciences) using a High Prime kit (Roche). Southern hybridization was performed using a conventional protocol. A 4.66-kb fragment and a 3.96-kb fragment were detected for the WT and targeted alleles, respectively.

Northern Blot Analysis—A Mouse Multiple Tissue Northern blot Membrane was purchased from Clontech. Total RNAs from mouse tissues were extracted using TRIzol reagent (Invitrogen) according to the manufacturer's instructions. Ten micrograms of total RNAs were separated by agarose gel electrophoresis and then transferred onto nylon membranes (GE Healthcare). Northern hybridization was performed with

TABLE 1
Primers used in this study

Allele or gene	Direction	Sequence (5′ → 3′)
For mouse genotyping		
Wild-type allele	Forward	ACAAAGAGCTACTAAGCACCTTG
	Reverse	TCAAAGACAGGCACTCTGTCAG
Targeted allele	Forward	GAATGAACTGCAGGACGAG
	Reverse	ACTAGAAGGCACAGTCGAG
For real-time PCR		
Rev7	Forward	GGGAAGGATGACCACCCTCACG
	Reverse	TCAGCTGTTCTTATGCGCTC
c-kit (37)	Forward	GCGTCCTGTTGGTCCTGCTCCGTG
	Reverse	CTTGCCGAGCTGATAGTCAGCGTC
Oct4 (36)	Forward	TTGGGCTAGAGAAGGATGTGGTT
	Reverse	GGAAAAGGGACTGAGTAGAGTGTGG
Blimp1	Forward	GTGAACGACCACCCCTGGGA
	Reverse	ACCGATGAGGGGTCCAAAGCG
Nanog	Forward	AGGGTCTGCTACTGAGATGCTCTG
	Reverse	CAACCACTGGTTTTTCTGCCACCG
Tiar	Forward	GGGGTCAGTGGTTGGGAGGT
	Reverse	GCCCCGAAGCAATTCCTCCAC
Cdc20	Forward	TCAAGGCGCTGTCAAGGCTGTGG
	Reverse	GCCACAACCGTAGAGTCTCA
Rev3	Forward	ACCTGGCTGCTGTCAAGTTCCG
	Reverse	TGTCAGCAGCTACGGCATCCAC
GAPDH	Forward	TGCACCACCAACTGCTTAG
	Reverse	GAGGCAGGGATGATGTTC

radiolabeled mouse *Rev7* or *β-actin* cDNA probes using standard methodologies.

Western Blot Analysis—Small pieces of mouse tissue were homogenized by sonication in SDS sample buffer (62.5 mM Tris-HCl, pH 6.8, 2% SDS, 25% glycerol, and 20 μg/ml of bromophenol blue). After measuring the protein concentration using a DC protein Assay Kit (Bio-Rad), lysates were boiled at 100 °C for 2 min in the presence of 2% 2-mercaptoethanol. Lysates containing 50 μg of protein were subjected to SDS-PAGE and then transferred onto PVDF membranes (Millipore Corporation). The membranes were blocked for 1 h at room temperature (RT) in Blocking One (Nacalai Tesque) with gentle agitation and then incubated with the primary antibody for 1 h at RT. After washing with TBST buffer (20 mM Tris-HCl, pH 7.6, 137 mM NaCl, and 0.1% Tween 20), membranes were incubated with the secondary antibody conjugated to HRP (Dako) for 1 h at RT. After washing the membranes, the reaction was detected using an ECL Detection Kit (GE Healthcare) and visualized by an ImageQuant LAS 4000 mini (GE Healthcare).

Antibodies—A rabbit polyclonal anti-REV7 antibody was produced by immunization with full-length human REV7 protein fused to GST. The antibody was affinity purified using full-length recombinant mouse REV7 protein. Anti-promyelocytic leukemia zinc finger protein (PLZF), -GATA-4, -Oct4, -proliferating cell nuclear antigen (PCNA), and -GAPDH antibodies were purchased from Santa Cruz Biotechnology. An anti-cleaved caspase-3 antibody was purchased from Cell Signaling Technology, Japan. Anti-phospho-histone H2A.X (Ser-139), -dimethyl-histone H3 (Lys-9), and -trimethyl-histone H3 (Lys-27) antibodies were purchased from Millipore Corporation.

Histological Analysis—Mouse tissues were fixed in 10% neutral-buffered formalin, dehydrated, and embedded in paraffin. Four-μm thick sections were prepared for H&E staining and immunohistochemistry. H&E staining was performed by a conventional method.

Immunohistochemistry—Sections were deparaffinized in xylene and rehydrated in a graded series of ethanol. For antigen retrieval, sections were immersed in Target Retrieval Solution, pH 9.0 (Dako), and heated for 30 min at 98 °C in a water bath. Nonspecific binding was blocked with 10% normal goat serum for 10 min at RT. Sections were then incubated with primary antibodies for 1 h at RT. Endogenous peroxidase was inhibited by incubation with 3% hydrogen peroxide in methanol for 15 min. Then, sections were incubated with the secondary antibody conjugated to HRP-labeled polymer (EnVision+ anti-rabbit; Dako) for 15 min at RT. The reaction products were visualized with diaminobenzidine (DAB) (Dako), and nuclei were counterstained with hematoxylin.

Whole Mount Immunohistochemistry—Whole mount immunohistochemistry was performed as described previously (35). Mouse embryos were fixed in 10% neutral-buffered formalin overnight, washed three times with PBST (10 mM phosphate-buffered saline, and 0.1% Tween 20, pH 7.4) for 10 min, washed three times with distilled water for 10 min, and then heated in Target Retrieval Solution for 30 min at 98 °C. Embryos were then washed three times with PBST for 10 min and then immersed in 10% normal rabbit serum for 90 min at RT for blocking. Samples were incubated with an anti-Oct4 antibody (1:100 dilution) overnight at 4 °C and then washed three times with PBST for 30 min. Endogenous peroxidase was inhibited by incubation with 2% hydrogen peroxide in TBST for 4 h at 4 °C. Then, samples were incubated with an anti-mouse IgG antibody conjugated to HRP-labeled polymer (1:200 dilution) (Dako) overnight at 4 °C, followed by washing 12 times with PBST for 30 min. The immunoreaction was visualized using DAB.

Real-time Quantitative RT-PCR—To obtain embryos, pregnant mice were anesthetized with sevoflurane prior to being sacrificed. Dissected organs (E17.5, ~30 mg), whole bodies (E8.5), or trunks (E13.5) were homogenized in RLT buffer of the RNeasy Mini Kit (Qiagen) using BioMasher (Nippi). Total RNA was isolated from the homogenate using the RNeasy Mini Kit, followed by treatment with DNase (Qiagen) to minimize genomic DNA contamination according to the manufacturer's protocol. Purified RNA samples were reverse-transcribed using ReverTra Ace (Toyobo). Twelve ng of RNA equivalent-cDNA was mixed with Thunderbird SYBR qPCR Mix (Toyobo) and amplified on a Mx3005P thermal cycler (Agilent Technologies) using gene-specific primer sets as described in Table 1 (36, 37).

In Situ Hybridization on Frozen Sections—Mice were perfused intravascularly with a 4% paraformaldehyde solution. The testes were dissected, embedded in OCT compound (Sakura Finetek), and then frozen on dry ice. Ten-micrometer thick sections were prepared using a cryostat (Leica Microsystems). A mouse *Rev7*-specific riboprobe was designed to target the 207-bp region that was deleted in the $Rev7^{-/-}$ mouse. A PCR product containing the riboprobe target region and RNA polymerase binding sites (SP6 for the sense probe, and T7 for the antisense probe) were generated using primers 5′-CCAAGCTATTTAGGTGACACTATAGAACACCCTCCACGCCCTCCC-3′ and 5′-TGAATTGTAATACGACTCACTATAGGGAGATCCGGGTGACAGGACACTGAA-3′. Radiolabeled riboprobes were synthesized with SP6 and T7 RNA

polymerases (Roche) and [^{33}P]dUTP (PerkinElmer Life Sciences). Sections were hybridized overnight at 60 °C using 200 μl of hybridization solution per section, consisting of 1×10^6 cpm of radiolabeled probe and hybridization buffer (50% formamide, 10% dextran sulfate, 0.5 M NaCl, 1× Denhardt's solution, 10 mM Tris, pH 8.0, 1 mM EDTA, 500 μg/ml of yeast tRNA, and 10 mM DTT). Following hybridization, sections were immersed in 2× standard saline citrate for 15 min at RT and then in RNase buffer (20 μg/ml of RNase A, 0.5 M NaCl, 10 mM Tris, pH 8.0, and 1 mM EDTA) for 30 min at 37 °C. After extensive washing and dehydration, sections were dipped in twice-diluted Kodak Autoradiography Emulsion, Type NTB (Eastman Kodak), and then dried at RT for 30 min in a darkroom. Sections were stored at 4 °C for ~2 weeks while protected from light and developed using Kodak D19 Developer and Fixer (Eastman Kodak).

Whole Mount in Situ Hybridization—Whole mount *in situ* hybridization was performed with digoxigenin (DIG)-labeled RNA probes as described previously (38). Probes were synthesized using the same PCR product used for *in situ* hybridization on frozen sections and DIG RNA labeling mix (Roche Applied Science). Mouse embryos were fixed overnight in 4% paraformaldehyde, treated with 10 μg/ml of proteinase K in PBST at 37 °C for 15 min, and then treated with 2 mg/ml of glycine at RT for 5 min. After re-fixation with 4% paraformaldehyde + 0.2% glutaraldehyde in PBST for 20 min at RT, embryos were immersed in pre-hybridization buffer (50% formamide, 5× SSC, 50 μg/ml of heparin, 5 mg/ml of trout RNA, 2% blocking reagent (Roche Applied Science), and 0.1% Tween 20) for 90 min at 70 °C, and then incubated with hybridization solution (0.2 μg of DIG-labeled RNA probes in pre-hybridization buffer) at 70 °C overnight. Following hybridization, samples were rinsed three times with washing buffer 1 (50% formamide, 5× SSC, and 0.1% Tween 20) at 70 °C for 30 min, and then three times with washing buffer 2 (50% formamide, 2× SSC, and 0.1% Tween 20) at 65 °C for 30 min. After blocking with 5% normal sheep serum for 90 min, embryos were incubated with an anti-DIG antibody conjugated to AP (1:10,000 dilution) at 4 °C overnight. Embryos were washed 10 times with PBST for 30 min, and the signals were visualized using BM purple AP substrate (Roche Applied Science).

Fluorescence Staining—For immunofluorescence staining, an Alexa Fluor 488- or 594-labeled secondary antibody (Invitrogen) was applied for 30 min at RT. The TUNEL assay was performed according to the manufacturer's instructions (*In Situ* Cell Death Detection Kit, Fluorescein; Roche). Images were obtained under a fluorescence microscope (Olympus).

Statistical Analysis—Statistical significance was determined with the Student's *t* test. A value of $p < 0.05$ was considered significant.

RESULTS

Generation of Rev7-Knock-out Mice—To generate mice lacking the *Rev7* transcript, a targeting vector was designed to delete the start codon located in exon 1–2 of the *Rev7* locus. This deletion was replaced by the *PGK-neo* cassette (Fig. 1*A*). ES cell clones with homologous recombination were injected into blastocysts. The resultant chimeric male mice were mated with C57BL/6 female mice to ascertain germ-line transmission of the targeted locus, and *Rev7* heterozygous knock-out ($Rev7^{+/-}$) mice were produced. $Rev7^{+/-}$ siblings were then intercrossed to produce homozygous knock-out ($Rev7^{-/-}$) mice. Genotyping of $Rev7^{+/+}$, $Rev7^{+/-}$, and $Rev7^{-/-}$ mice by Southern blotting using a 5′ probe showed a single band of 4.66 kb for $Rev7^{+/+}$ mice, a single band of 3.96 kb for $Rev7^{-/-}$ mice, and both bands for $Rev7^{+/-}$ mice (Fig. 1*B*). PCR genotyping using genomic DNAs and primers specific for WT and knock-out alleles showed a 230-bp band and a 750-bp band, and both bands for $Rev7^{+/+}$, $Rev7^{-/-}$, and $Rev7^{+/-}$ mice, respectively (Fig. 1*C*). Northern blot analysis using RNAs extracted from the testes of $Rev7^{+/+}$ and $Rev7^{-/-}$ mice showed a 1.3-kb band for $Rev7^{+/+}$ mice and no band for $Rev7^{-/-}$ mice (Fig. 1*D*). In addition, Western blot analysis with the anti-REV7 antibody using lysates prepared from the testes, kidneys, liver, and spleen of $Rev7^{+/+}$ and $Rev7^{-/-}$ mice showed high levels of REV7 protein in the testes and low levels in the liver of $Rev7^{+/+}$ mice, and a complete absence of REV7 in all the tissues of $Rev7^{-/-}$ mice (Fig. 1*E*). These results confirmed the establishment of *Rev7*-knock-out mice that were null for REV7 expression.

High Level of REV7 Expression in Germ Cells of the Testis—The tissue distribution of REV7 expression was analyzed at mRNA and protein levels. *Rev7* mRNA distribution was analyzed by Northern blotting using a Multiple Tissue Northern blot membrane, revealing that *Rev7* was expressed in the heart, liver, kidney, and most predominantly in the testis (Fig. 2*A*). REV7 protein distribution was analyzed by Western blotting with the anti-REV7 antibody using lysates extracted from various organs of postnatal day 56 (P56) WT mice. A high level of REV7 protein was also detected in the testis, and a low level of REV7 protein was present in the ovary. However, REV7 was almost undetectable in other organs (Fig. 2*B*).

Next, we analyzed in detail the expression of REV7 in the testis. *Rev7* mRNA was assessed by *in situ* hybridization using *Rev7* antisense and sense probes and sections of P56 WT testis. The antisense *Rev7* probe produced strong signals in the seminiferous tubules with stronger signals in the peripheral region (Fig. 2*C*). The sense *Rev7* probe produced no signals, indicating that *Rev7* is specifically expressed in the seminiferous tubules. REV7 protein was analyzed by immunohistochemical and immunofluorescence staining using the anti-REV7 antibody. REV7 protein was clearly detected in a wide range of cells in the seminiferous tubules, and especially in spermatogonia and spermatocytes (Fig. 2*D*). However, its level was comparatively low in spermatozoa and almost undetectable in Sertoli cells. REV7 protein was localized mainly in the nucleus. These findings from *in situ* hybridization and immunostaining suggest that REV7 plays an important role in germ cell biology.

REV7 Expression Is Ubiquitously Detected in the Mouse Embryo and Becomes Confined to the Testis after Birth—Next, we evaluated REV7 expression during embryonic, newborn, and young adult periods. Using E9.5 WT mouse embryos, *Rev7* mRNA was examined by whole mount *in situ* hybridization using *Rev7* antisense and sense probes. The antisense probe detected a positive signal throughout the entire body (*purple* signal), whereas no signal was detected using the sense probe (Fig. 2*E*, *upper panels*). *In situ* hybridization on a tissue section

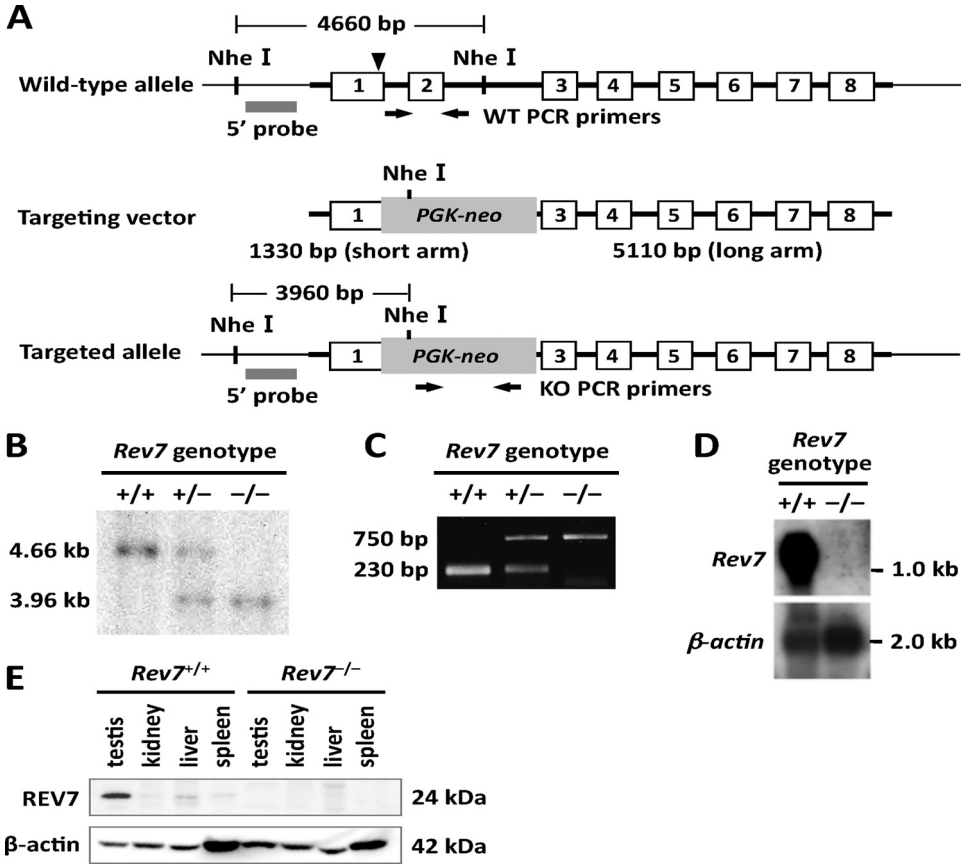

FIGURE 1. **Establishment of the *Rev7*-knock-out mouse.** *A*, homologous recombination strategy to generate $Rev7^{-/-}$ mice. The genomic sequence containing *Rev7* exon 1 (including the start codon) and exon 2 was replaced by a neomycin cassette. Positions of the 5′ probe for Southern blot screening (*gray bars*) and PCR primers (*arrows*) for WT and targeted alleles to screen mouse genotypes are shown. *Arrowhead* indicates the position of the start codon. *B*, genotyping of $Rev7^{+/+}$, $Rev7^{+/-}$, and $Rev7^{-/-}$ mice by Southern blotting. Genomic DNAs extracted from mouse tails were digested with NheI and Southern hybridization was performed using the ^{32}P-labeled 5′ probe. The 4.66- and 3.96-kb bands represent WT and targeted alleles, respectively. *C*, genotyping of $Rev7^{+/+}$, $Rev7^{+/-}$, and $Rev7^{-/-}$ mice by PCR. The 230- and 750-bp bands represent WT and targeted alleles, respectively. *D*, Northern blot analysis of total RNA extracted from the testes of $Rev7^{+/+}$ and $Rev7^{-/-}$ mice. ^{32}P-Labeled full-length *Rev7* cDNA was used as the probe (*upper panel*). Blotting for *β-actin* expression is shown as the internal control (*bottom panel*). *E*, Western blot analysis to detect REV7 protein in tissues of $Rev7^{+/+}$ and $Rev7^{-/-}$ mice (*upper panel*). Lysates were prepared from testes, kidneys, liver, and spleen of $Rev7^{+/+}$ and $Rev7^{-/-}$ mice. Detection of β-actin is shown as the internal control (*bottom panel*).

of E9.5 WT embryos was also performed. A positive signal was detected throughout the body, especially in the periventricular area, by using the antisense probe (Fig. 2*E*, *lower panels*). We checked *Rev7* expression in a late embryonic stage (E17.5) by real-time quantitative RT-PCR, in which *Rev7* mRNA expression was detected in all the analyzed organs with high level expression in the cerebrum and cerebellum (Fig. 2*F*). These results indicate that *Rev7* is expressed not only in germ cells but also in somatic cells at an embryonic stage. On the other hand, during newborn and young adult periods, REV7 expression was clearly detected in the testis at all ages, whereas REV7 gradually diminished with age in other organs analyzed by Western blotting (Fig. 2*G*). These results indicate that REV7 is expressed in a wide range of cells during embryonic stages and its expression subsequently becomes confined to the testis after birth.

$Rev7^{-/-}$ Mice Are Partially Embryonic Lethal—After $Rev7^{+/-}$ male and female mice were intercrossed to generate $Rev7^{-/-}$ mice, we observed that $Rev7^{-/-}$ mice were born but the number of $Rev7^{-/-}$ mice was fewer than expected according to the Mendelian ratio (Table 2). When we checked the numbers of $Rev7^{+/+}$, $Rev7^{+/-}$, and $Rev7^{-/-}$ embryos from E8.5 to E13.5, they were mostly compatible with the expected Mendelian ratios (Table 2). These findings indicate that $Rev7^{-/-}$ mice are partially embryonic lethal with some surviving to birth.

REV7 Deficiency Results in a Congenital Spermatogonia Defect in Living Male Mice—$Rev7^{+/-}$ mice were fertile and showed no obvious differences compared with that of WT mice. The $Rev7^{-/-}$ mice that were born looked feeble, and their body size was small compared with that of $Rev7^{+/+}$ or $Rev7^{+/-}$ littermates (Fig. 3*A*). The body size of $Rev7^{-/-}$ mouse embryos was also small (Fig. 3*B*). The body weight of $Rev7^{-/-}$ male mice was significantly lower than that of $Rev7^{+/+}$ or $Rev7^{+/-}$ mice (Fig. 3*D*). $Rev7^{-/-}$ male mice were infertile, and their testes were quite small compared with those of $Rev7^{+/+}$ siblings (Fig. 3*C*). The ratio of testis to body weight of $Rev7^{-/-}$ mice was significantly lower than that of $Rev7^{+/+}$ mice, whereas the ratio of heart to body weight of $Rev7^{-/-}$ mice was not significantly different from that of $Rev7^{+/+}$ mice (Fig. 3*E*). Histological analysis revealed that the seminiferous tubules of the testes of $Rev7^{-/-}$ mice were entirely atrophic at P14 and P56, which contained very few cells in the peripheral region and no spermatozoa, whereas numerous germ cells and spermatozoa were present in the seminiferous tubules of $Rev7^{+/+}$ siblings (Fig.

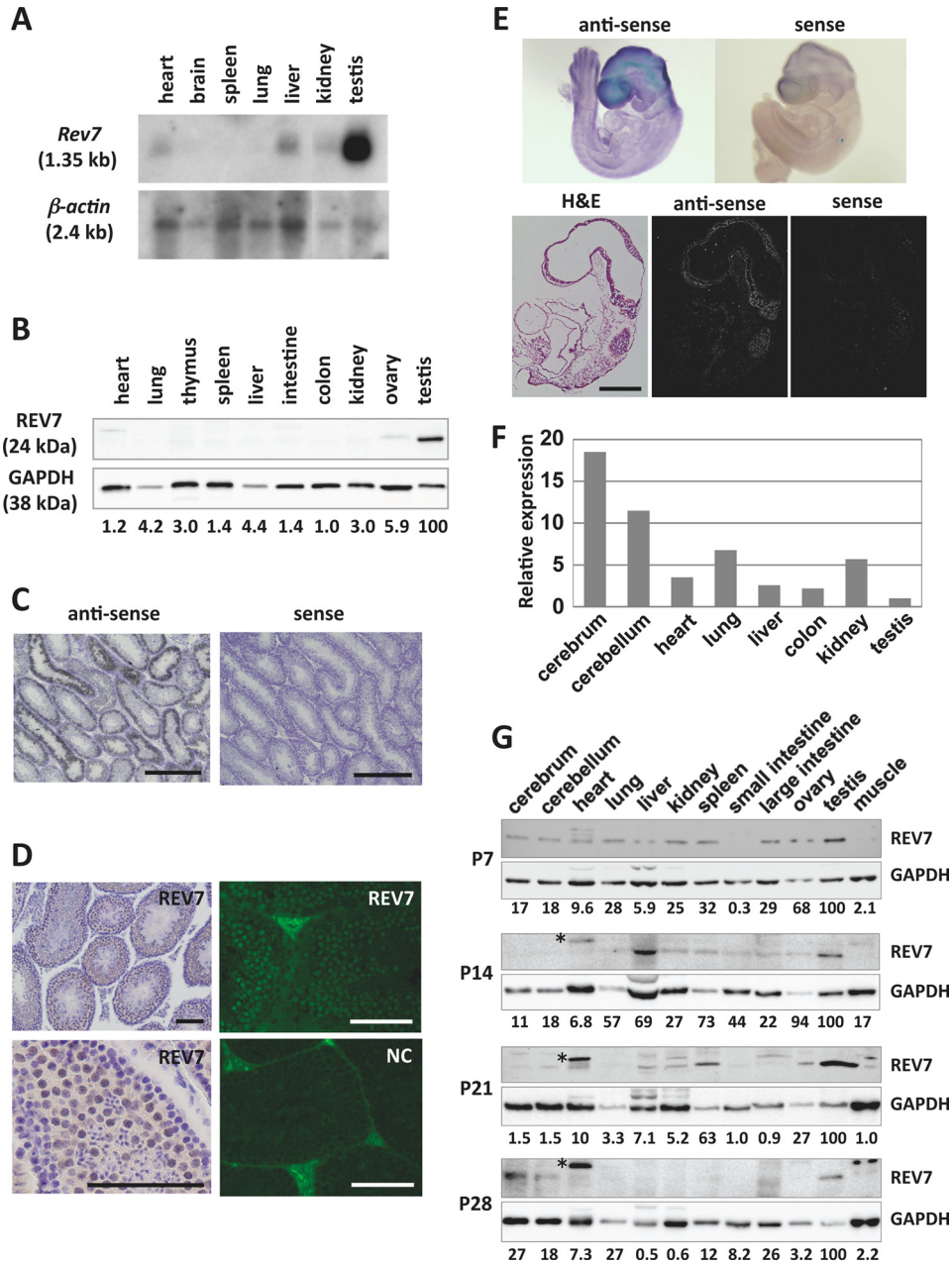

FIGURE 2. ***Rev7* expression in WT mice.** *A,* Northern blot analysis of *Rev7* expression. A Mouse Multiple Tissue Northern blot membrane was hybridized with the ^{32}P-labeled *Rev7* cDNA probe (*upper panel*). A blot hybridized with the *β-actin* cDNA probe is shown as the internal control (*bottom panel*). *B,* Western blot analysis of REV7 expression. Lysates were prepared from P56 WT mice, and Western blotting was performed using the anti-REV7 antibody. REV7 expression was quantitatively assessed using ImageQuant TL, which is indicated at the *bottom*. *C*, *in situ* hybridization to detect the *Rev7* transcript in the testis. ^{33}P-Labeled antisense and sense probes for the *Rev7* transcript were used for *in situ* hybridization on testis sections of P56 WT mice. *Scale bars*, 500 *μ*m. *D,* immunohistochemical staining for REV7 expression in the testis. Immunostaining was performed with the anti-REV7 antibody on testis sections from P56 WT mice. Positive signals were visualized with DAB or a fluorescently labeled secondary antibody. Immunofluorescence staining without the primary antibody is shown as the negative control (*NC*). *Scale bars*, 100 *μ*m. *E*, *in situ* hybridization using whole embryonic tissues (*upper panels*) and tissue sections (*bottom panels*) to detect *Rev7* expression in E9.5 embryos. Whole mount *in situ* hybridization was performed with DIG-labeled antisense and sense probes for the *Rev7* transcript and *in situ* hybridization on tissue sections was performed with ^{33}P-labeled probes as described under "Experimental Procedures." In the whole mount *in situ* hybridization, the *purple* color throughout the body represents a specific signal (*upper left panel*). A H&E-stained image of the tissue section is also shown (*bottom left panel*). *Scale bar*, 500 *μ*m. *F*, real-time quantitative RT-PCR analysis of *Rev7* expression in E17.5 embryos. Total RNAs were extracted from the indicated organs. Real-time quantitative RT-PCR was performed using gene-specific primers for *Rev7* and *GAPDH* transcripts listed in Table 1. Relative expression of the *Rev7* transcript in each organ is graphically shown. Reactions for *GAPDH* are used as internal controls. *G*, Western blot analysis of REV7 at postnatal stages. Lysates were prepared from the indicated organs, and Western blot analysis was performed with anti-REV7 and anti-GAPDH antibodies. Relative expression of REV7 was quantitatively assessed using ImageQuant TL, which is indicated at the *bottom* of each panels. The bands indicated by *asterisks* are nonspecific.

3*F*). To understand why spermatogenesis did not occur in *Rev7*$^{-/-}$ testes, we performed immunohistochemical analyses using the anti-PLZF antibody that is specific for spermatogonia. As shown in Fig. 3*G*, some PLZF-positive spermatogonia were identified in the basal region of the seminiferous tubules of *Rev7*$^{+/+}$ mice at P0 and P14. In contrast, no PLZF-positive spermatogonia were identified in the seminiferous tubules of *Rev7*$^{-/-}$ mice (Fig. 3*G*). Analysis using the anti-GATA-4 anti-

TABLE 2
Numbers (%) of mice obtained from *Rev7*$^{+/-}$ mice intercross

Stage	Genotype			Total
	Rev7$^{+/+}$	*Rev7*$^{+/-}$	*Rev7*$^{-/-}$	
E8.5-E13.5	33 (26.0)	64 (50.4)	30 (23.6)	127 (100)
After birth	65 (34.4)	106 (56.1)	18 (9.5)	189 (100)

body, which is specific for Sertoli cells, showed that all of the cells in the seminiferous tubules of *Rev7*$^{-/-}$ mice were GATA-4-positive Sertoli cells (Fig. 3*G*). These findings indicate a congenital spermatogonial defect in *Rev7*$^{-/-}$ mice, which results in an absence of spermatogenesis, thereby retaining only Sertoli cells in the seminiferous tubules.

REV7 Deficiency Also Impairs Oogenesis in Female Mice—The body size of *Rev7*$^{-/-}$ female mice, which were also infertile, was significantly smaller, compared with that of *Rev7*$^{+/+}$ and *Rev7*$^{+/-}$ siblings (Fig. 4*A*). Macroscopically, the ovaries of *Rev7*$^{-/-}$ female mice were quite small and atrophic compared with those of *Rev7*$^{+/+}$ siblings (Fig. 4*B, left panels*). Histopathologically, the ovaries of adult *Rev7*$^{+/+}$ mice at P28 had many follicles containing oocytes, whereas those of *Rev7*$^{-/-}$ mice consisted of stromal and epithelial cells without follicles (Fig. 4*B*, *middle* and *right panels*). We checked *Rev7* mRNA expression in WT mouse ovary by *in situ* hybridization, in which the antisense probe detected an elevated signal in the oocyte, demonstrating *Rev7* expression in the oocyte (Fig. 4*C*). These results indicate that REV7 deficiency causes germ cell aplasia in both male and female mice.

Apoptotic Cell Death of PGCs during Migration in REV7-deficient Embryos—Because *Rev7*$^{-/-}$ germ cells were not present in either sex, we hypothesized that REV7 deficiency causes developmental abnormalities in PGCs during early embryonic stages before sexual differentiation. To ascertain the development of PGCs at early embryonic stages, we performed whole mount immunohistochemistry with the anti-Oct4 antibody on *Rev7*$^{+/+}$ and *Rev7*$^{-/-}$ mouse embryos to identify PGCs. At E8.5, PGCs were clearly identified at the base of the allantois in *Rev7*$^{-/-}$ mouse embryos, indicating no obvious difference in the number of PGCs from that in *Rev7*$^{+/+}$ mouse embryos (Fig. 5*A*, *left panels*). During E9.5–10.5, migrating PGCs were detected in *Rev7*$^{-/-}$ mice, but the number of PGCs progressively decreased with time (Fig. 5*A*, *middle* and *right panels*). After E11.5, the presence of PGCs was assessed by immunohistochemical staining of tissue sections with the anti-Oct4 antibody. At E11.5, the majority of PGCs in *Rev7*$^{-/-}$ mice had disappeared and only a few PGCs were detected around the genital ridges (Fig. 5*B*, *left panels*). At E13.5, PGCs in *Rev7*$^{-/-}$ mice were completely undetectable at the genital ridges (Fig. 5*B*, *middle panels*). These results suggest that REV7 deficiency does not affect the development or migration of PGCs, but causes progressive loss of migrating PGCs during E9.5–13.5. Next, cleaved caspase-3 immunoreactivity was assessed using serial tissue sections of E11.5 embryos, in which cleaved caspase-3-positive cells were detected at a high frequency around the genital ridges of *Rev7*$^{-/-}$ mice compared with that of *Rev7*$^{+/+}$ mice (Fig. 5*B*, *right panels*), and some cells were positive for both Oct4 and cleaved caspase-3, suggesting apoptosis of PGCs (Fig. 5*B*, *arrows*). We also performed double fluorescence staining for Oct4 and TUNEL using tissue sections around the hindgut of E9.5 embryos to confirm apoptosis of PGCs (Fig. 5*C*). We found that some of the Oct4-positive PGCs were TUNEL positive in *Rev7*$^{-/-}$ mice (Fig. 5*C, arrowheads*), whereas none of the Oct4-positive PGCs were TUNEL positive in *Rev7*$^{+/+}$ mice, indicating that REV7 deficiency causes apoptotic cell death of PGCs during embryonic stages. We checked REV7 expression in PGCs by double immunostaining with anti-REV7 and anti-Oct4 antibodies using tissue sections of the genital ridge of E13.5 WT embryos. REV7 expression was detected in most of the cells in the genital ridge, and some of which were Oct4-positive PGCs (Fig. 5*D*). These results indicate that REV7 is expressed in PGCs and plays an essential role in the survival of PGCs in mouse embryos.

REV7 Deficiency Causes Increased Apoptotic Cell Death in the Neuroblasts of Mouse Embryos but Does Not Affect Cell Proliferation—We further evaluated cleaved caspase-3-positive apoptotic cells among neuroblasts in the forebrain of E11.5 embryos, in which the frequency of apoptotic cells significantly increased in *Rev7*$^{-/-}$ embryos (Fig. 6, *A* and *B*), indicating that REV7 deficiency causes apoptotic cell death not only in PGCs but also in the somatic cells of embryos. We also assessed cell proliferation in the forebrain by immunohistochemical staining with the anti-PCNA antibody, but no significant difference was detected between *Rev7*$^{+/+}$ and *Rev7*$^{-/-}$ embryos (Fig. 6, *C* and *D*), suggesting that REV7 deficiency does not affect cell proliferation.

REV7 Deficiency Results in DNA Damage Accumulation and Elevated Levels of Histone Methylation—To investigate the cause of increased apoptotic cell death in *Rev7*$^{-/-}$ embryos, accumulation of DNA damage represented by double strand breaks, which can be detected by anti-phospho-H2AX (pH2AX) antibody, was assessed in *Rev7*$^{+/+}$ and *Rev7*$^{-/-}$ embryos by immunohistochemical staining. *Rev7*$^{-/-}$ embryos at E9.5 displayed a number of cells positive for pH2AX, some of which were also positive for Oct4, whereas pH2AX-positive cells were undetectable in the *Rev7*$^{+/+}$ embryo (Fig. 7*A*). In the *Rev7*$^{-/-}$ embryo at E13.5, when PGCs completely disappeared in *Rev7*$^{-/-}$ embryos, many somatic cells around the genital ridge appeared to be positive for pH2AX (Fig. 7*B*). These results indicate that REV7 deficiency causes DNA damage accumulation in both PGCs and somatic cells during the embryonic period. In addition, histone methylation represented by H3K9me2 and H3K27me3 were assessed in *Rev7*$^{+/+}$ and *Rev7*$^{-/-}$ embryos by immunofluorescence staining. Elevated levels of H3K9me2 and H3K27me3 were demonstrated in most cells of the *Rev7*$^{-/-}$ embryo at E9.5 compared with the *Rev7*$^{+/+}$ embryo (Fig. 7*A*). However, in embryos at E13.5, no obvious difference was detected in H3K9me2 and H3K27me3 levels between *Rev7*$^{+/+}$ and *Rev7*$^{-/-}$ embryos (Fig. 7*B*). These results indicate that REV7 deficiency also affects histone methylation levels at the early embryonic stage.

Deregulation of Gene Expression in REV7-deficient Embryos at E8.5—To elucidate the effect of REV7 deficiency on gene expression important for PGC survival, real-time quantitative RT-PCR was performed using RNAs extracted from *Rev7*$^{+/+}$ and *Rev7*$^{-/-}$ whole embryos at E8.5, when PGCs were present in *Rev7*$^{-/-}$ embryos, such as in *Rev7*$^{+/+}$ embryos (Fig. 5*A*), and

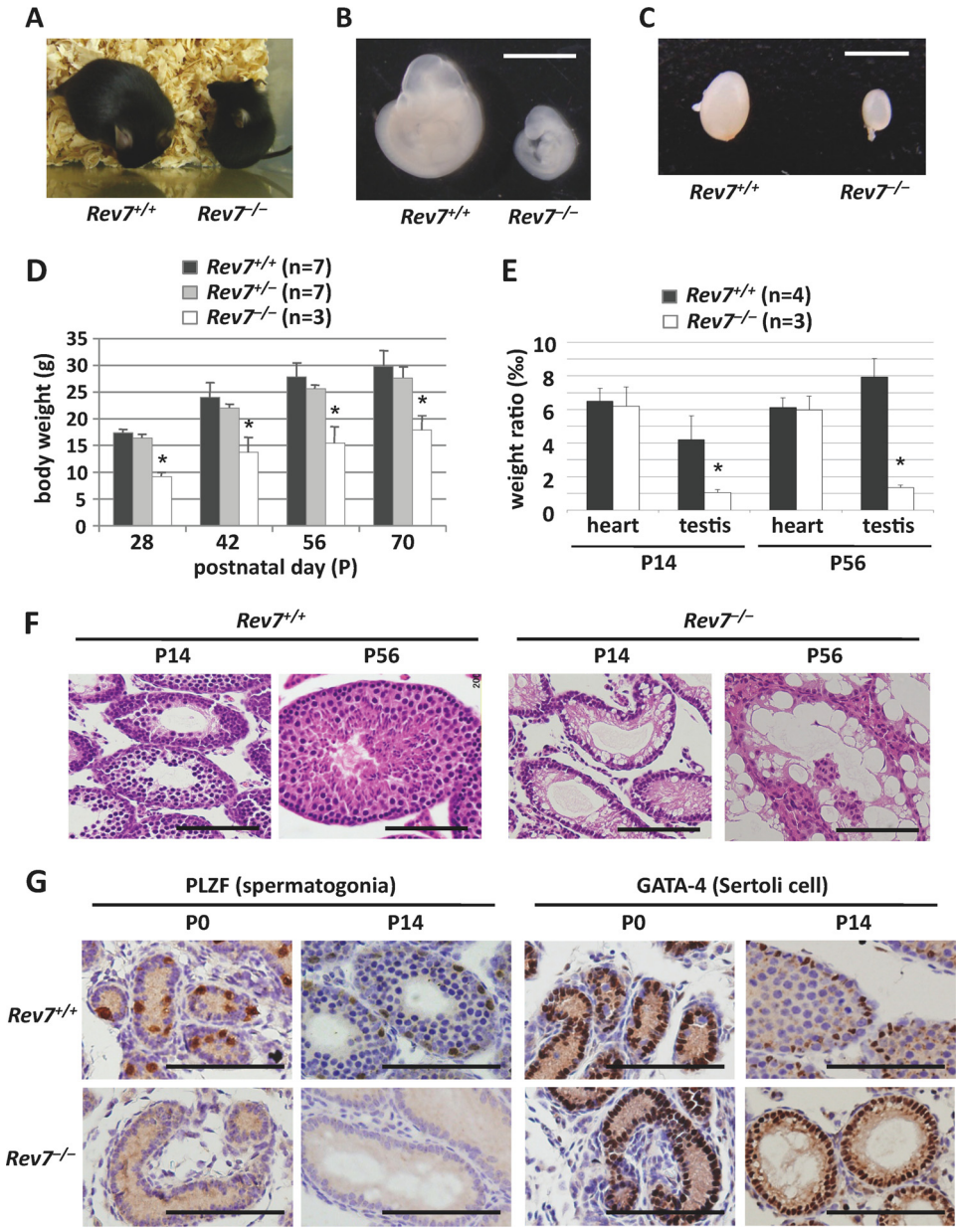

FIGURE 3. **Growth retardation and germ cell aplasia of *Rev7*$^{-/-}$ male mice.** *A* and *B*, gross appearance of *Rev7*$^{+/+}$ and *Rev7*$^{-/-}$ mice at P28 (*A*) and E10.5 (*B*). *Scale bar*, 3 mm. *C*, gross appearance of the testes of *Rev7*$^{+/+}$ and *Rev7*$^{-/-}$ mice at P7. *Scale bar*, 5 mm. *D*, comparison of the body weight of *Rev7*$^{+/+}$, *Rev7*$^{+/-}$, and *Rev7*$^{-/-}$ male mice. Mean ± S.D. are indicated. *Asterisks* indicate a significant difference ($p < 0.005$) between *Rev7*$^{-/-}$ mice and *Rev7*$^{+/+}$ or *Rev7*$^{+/-}$ mice. *E*, comparison of testis size between *Rev7*$^{+/+}$ and *Rev7*$^{-/-}$ mice. Mean ± S.D. of the ratios of heart to body weight and testis to body weight at P14 and P56 are indicated. *Asterisks* indicate a significant difference ($p < 0.001$) between *Rev7*$^{+/+}$ and *Rev7*$^{-/-}$ mice. *F*, histological images of the testes of *Rev7*$^{+/+}$ and *Rev7*$^{-/-}$ mice. Testis sections prepared from *Rev7*$^{+/+}$ and *Rev7*$^{-/-}$ mice at P14 and P56 were stained with H&E. *Scale bars*, 200 μm. *G*, immunohistochemical analysis of testis sections from *Rev7*$^{+/+}$ and *Rev7*$^{-/-}$ mice. Immunohistochemical staining with the anti-PLZF antibody for spermatogonia and the anti-GATA-4 antibody for Sertoli cells are indicated. *Scale bars*, 100 μm.

the expression of *Blimp1*, *Oct4*, *Nanog*, *c-Kit*, and *Tiar* was analyzed. As shown in Fig. 8*A*, *Oct4* and *Nanog* expression was up-regulated in *Rev7*$^{-/-}$ embryos compared with those in *Rev7*$^{+/+}$ embryos, whereas *Blimp1*, *c-Kit*, and *Tiar* expression did not show an obvious association with *Rev7* status. We also analyzed the expression of *Cdc20* and *Rev3*, whose products interact with REV7, in which no association was detected between their expression and the *Rev7* status (Fig. 8*A*). Transcript expression of these genes in *Rev7*$^{+/+}$ and *Rev7*$^{-/-}$ embryos at E13.5 was also analyzed. It was revealed that *Oct4* expression was down-regulated in *Rev7*$^{-/-}$ embryos, whereas no obvious association was observed between the expression of other genes and the *Rev7* status (Fig. 8*B*). It was speculated that down-regulation of *Oct4* expression in *Rev7*$^{-/-}$ embryos may be due to lack of PGCs. These findings suggest that REV7 is involved in the expression of several genes including *Oct4* and *Nanog* in mouse embryos.

DISCUSSION

Infertility is a major problem for public health and ~15% of couples worldwide suffer from infertility (39, 40). Many genes involved in the regulation of male and female reproduction

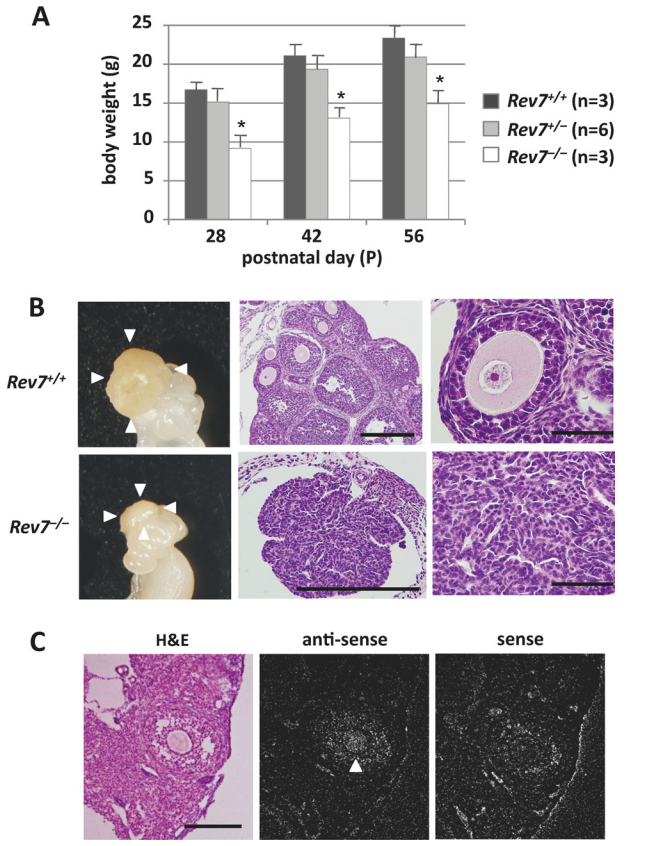

FIGURE 4. **Growth retardation and germ cell aplasia of *Rev7*$^{-/-}$ female mice.** *A,* comparison of the body weight of *Rev7*$^{+/+}$, *Rev7*$^{+/-}$, and *Rev7*$^{-/-}$ female mice. Mean ± S.D. are shown. *Asterisks* indicate a significant difference ($p < 0.005$) between *Rev7*$^{-/-}$ mice and *Rev7*$^{+/+}$ or *Rev7*$^{+/-}$ mice. *B,* gross appearances and histological images of the ovaries from *Rev7*$^{+/+}$ and *Rev7*$^{-/-}$ mice. Macroscopic images of the ovaries at P70 (*left panels*) and microscopic images of H&E-stained sections of the ovaries at P28 were shown (*middle panels*). *Right panels* are high magnification images. *Scale bars*, 200 μm (*middle panels*) and 50 μm (*right panels*). *C, in situ* hybridization to detect the *Rev7* transcript in the ovary. ^{33}P-Labeled antisense and sense probes for the *Rev7* transcript were used for *in situ* hybridization on ovary sections of a 18-week-old WT mouse. *Scale bar*, 200 μm.

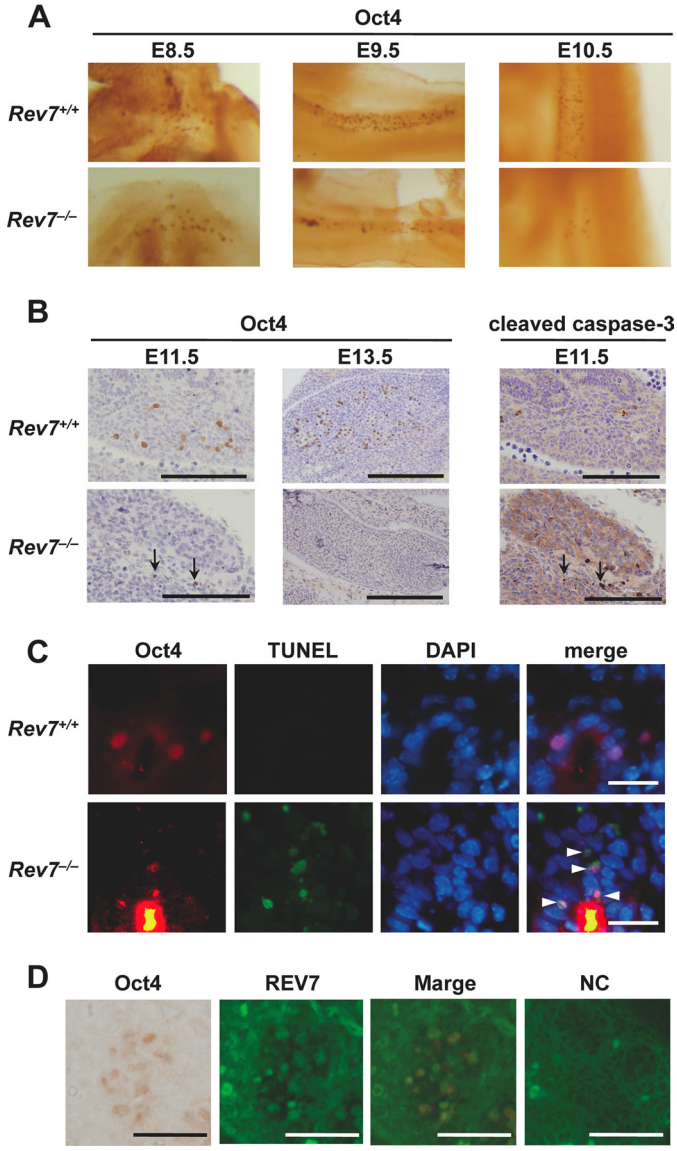

FIGURE 5. **Apoptotic cell death of PGCs during migration in *Rev7*$^{-/-}$ embryos.** *A,* immunohistochemical analysis of whole mount mouse embryos to identify PGCs during migration. *Rev7*$^{+/+}$ and *Rev7*$^{-/-}$ embryos at E8.5, E9.5, and E10.5 were whole mount immunostained using the anti-Oct4 antibody as described under "Experimental Procedures." Images were obtained under a stereomicroscope. *B,* immunohistochemical analysis of paraffin sections to detect PGCs and apoptotic cells. Sections around the genital ridges of *Rev7*$^{+/+}$ and *Rev7*$^{-/-}$ embryos at E11.5 and E13.5 were immunostained with the anti-Oct4 antibody to detect PGCs (*left* and *middle panels*). Those of *Rev7*$^{+/+}$ and *Rev7*$^{-/-}$ embryos at E11.5 were immunostained with the anti-cleaved caspase-3 antibody to detect apoptotic cells (*right panels*). Sections of E11.5 embryos used for Oct4 and cleaved caspase-3 staining (*left* and *right panels*) were serial sections. *Arrows* indicate cells positive for both Oct4 and cleaved caspase-3. *Scale bars*, 100 μm (*left* and *right panels*) and 200 μm (*middle panels*). *C,* fluorescence staining to demonstrate PGC apoptosis. Sections around the hindgut of *Rev7*$^{+/+}$ and *Rev7*$^{-/-}$ mouse embryos at E9.5 were subjected to immunostaining with the anti-Oct4 antibody, TUNEL staining, and nuclear staining with DAPI. Merged images are also shown. *Arrowheads* indicate cells positive for both Oct4 and TUNEL. *Scale bars*, 25 μm. *D,* REV7 expression in the PGCs of E13.5 embryos. Sections of genital ridges of E13.5 WT embryos were double immunostained with anti-Oct4 and anti-REV7 antibodies. Immunoreactivity of the anti-Oct4 antibody was visualized with DAB and that of the anti-REV7 antibody was visualized using an Alexa Fluor 488-labeled secondary antibody. The two images were merged after conversion of the DAB color to *red*. Immunofluorescence staining without the primary antibody is shown as the negative control (*NC*). *Scale bars*, 50 μm.

have been identified in mice, and some genetic causes for male and female infertility have been identified in humans, including chromosomal aberrations and genetic alterations of genes involved in sex determination, endocrinopathies, and sperm production (41, 42). However, many cases are still diagnosed with idiopathic infertility, and most of these cases are thought to have undiscovered genetic and epigenetic alterations.

REV7 is involved in DNA damage tolerance, cell cycle regulation, gene expression, and carcinogenesis by regulating the function of its interaction partners (19–21, 23, 27–31). However, the significance of Rev7 in mouse development has not been investigated. In the present study, we have demonstrated that *Rev7*$^{-/-}$ mice display a loss of PGCs by apoptotic cell death during migration, and germ cell aplasia in both testes and ovaries after birth, resulting in infertility of both sexes. These findings indicate that REV7 is essential for PGC survival in the mouse embryo. We hypothesized that DNA damage accumulation due to impairment of the DNA repair system or deregulation of the expression of specific genes necessary for PGC survival is likely to be the cause of PGC loss in *Rev7*$^{-/-}$ embryos. Consequently, we analyzed the frequency of cells with

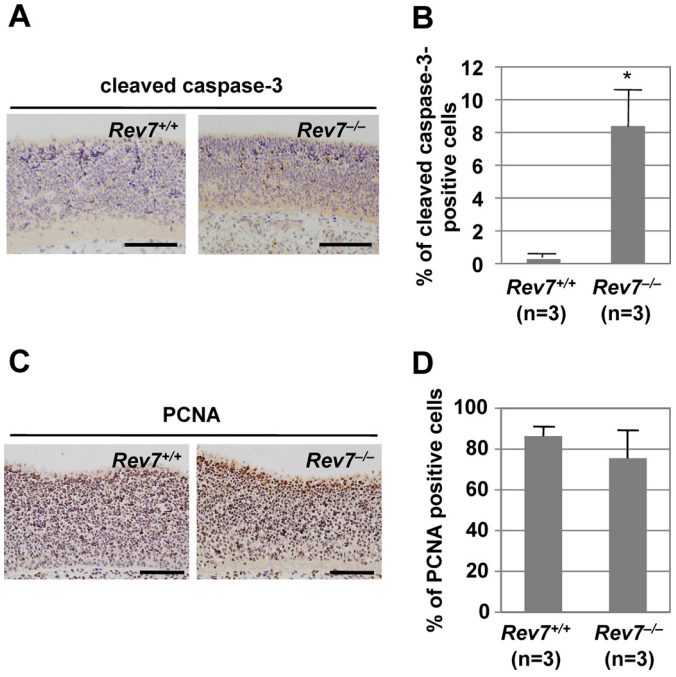

FIGURE 6. **REV7 deficiency increases the number of apoptotic cells among forebrain neuroblasts but does not affect cell proliferation.** *A,* detection of apoptotic cells in the forebrain. Sections of the forebrain of *Rev7*$^{+/+}$ and *Rev7*$^{-/-}$ mouse embryos at E11.5 were immunostained with the anti-cleaved caspase-3 antibody. *Scale bars*, 200 μm. *B,* percentages of cleaved caspase-3-positive cells (mean ± S.D.) among the forebrain neuroblasts of *Rev7*$^{+/+}$ and *Rev7*$^{-/-}$ embryos shown in *A*. An *asterisk* indicates a significant difference between *Rev7*$^{+/+}$ and *Rev7*$^{-/-}$ embryos ($p < 0.05$). *C*, analysis of cell proliferation in the forebrain. Sections of the forebrain of *Rev7*$^{+/+}$ and *Rev7*$^{-/-}$ mouse embryos at E11.5 were immunostained with the anti-PCNA antibody. *Scale bars*, 200 μm. *D,* percentages of PCNA cells (mean ± S.D.) among the forebrain neuroblasts of *Rev7*$^{+/+}$ and *Rev7*$^{-/-}$ embryos shown in *C*.

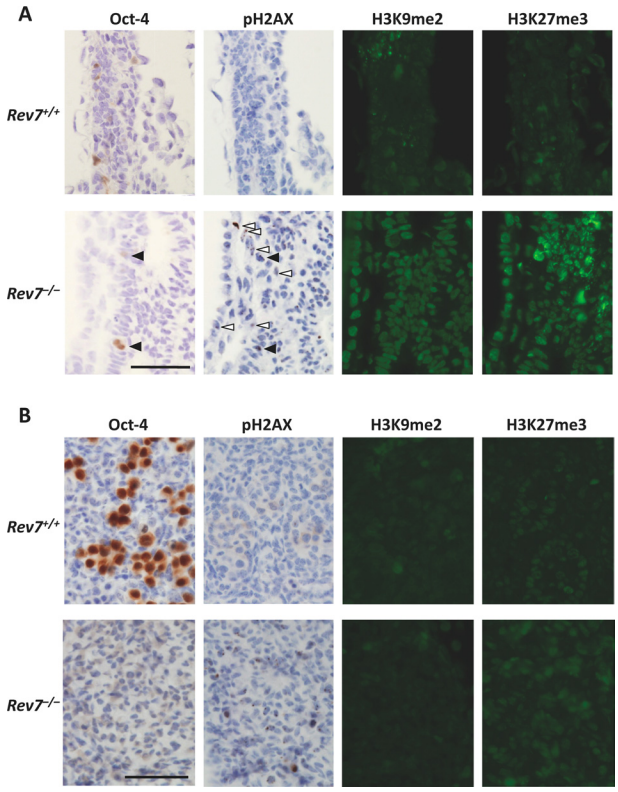

FIGURE 7. **REV7 deficiency results in DNA damage accumulation and increased levels of histone methylation in mouse embryos.** *A* and *B,* tissue sections around the hindgut of *Rev7*$^{+/+}$ and *Rev7*$^{-/-}$ mouse embryos at E9.5 (*A*) and around the genital ridges at E13.5 (*B*) were subjected to immunostaining with the anti-Oct4, -phospho-histone H2A.X (Ser-139) (pH2AX), -dimethyl histone H3 (Lys-9) (H3K9me2), and -trimethyl histone H3 (Lys-27) (H3K27me3) antibodies. Immunoreactivity of the anti-Oct4 and -pH2AX antibodies was visualized with DAB and that of the anti-H3K9me2 and -H3K27me3 antibodies was visualized using an Alexa Fluor 488-labeled secondary antibody. Serial sections were used for staining of E9.5 embryos (*A*). *Open arrowheads* in *A* indicate cells positive for pH2AX, and *closed arrowheads* in *A* indicate cells positive for both Oct4 and pH2AX. A number of pH2AX-positive cells were detected in *Rev7*$^{-/-}$ mouse embryos at E9.5 and E13.5. In addition, increased levels of H3K9me2 and H3K27me3 were demonstrated in *Rev7*$^{-/-}$ embryos at E9.5, but not in those at E13.5. *Scale bars*, 50 μm.

DNA damage of double strand breaks, and found that a number of cells with DNA damage were detectable not only in PGCs but also in somatic cells of *Rev7*$^{-/-}$ embryos, whereas they were almost undetectable in *Rev7*$^{+/+}$ embryos (Fig. 7). This finding suggests that DNA damage accumulation and genetic instability may be a possible cause of apoptotic cell death of PGCs in *Rev7*$^{-/-}$ embryos. We also analyzed histone methylation of H3K9me2 and H3K27me3 and expression of some essential genes for PGC survival. We found that H3K9me2 and H3K27me3 were enhanced in *Rev7*$^{-/-}$ embryos at E9.5 (Fig. 7*A*) and *Oct4* and *Nanog* expression was up-regulated in *Rev7*$^{-/-}$ embryos at E8.5 (Fig. 8*A*). H3K9me2 and H3K27me3 are principal epigenetic modifications in PGCs to control the chromatin state and gene expression (14, 15). Both Oct4 and Nanog are essential transcription factors for PGCs during migration and are required for the maintenance of PGC pluripotency (13, 43–45). Therefore, there is a possibility that deregulation of the expression of several genes in PGCs caused by Rev7 deficiency results in PGC apoptosis during migration, although more genes involved in PGC survival remain to be elucidated.

In this study, we found that *Rev7*$^{-/-}$ embryos exhibited a reduced body size, partial embryonic lethality, increased numbers of apoptotic somatic cells, and a high frequency of DNA damaged somatic cells, suggesting that *Rev7* is necessary for the maintenance of somatic cells as well as germ cells in the mouse embryo, and that partial embryonic lethality of *Rev7*$^{-/-}$ mice may possibly be due to the numerous apoptotic cell death in somatic cells caused by DNA damage accumulation. It has been reported that REV7 interacts with REV3 forming Pol ζ, a DNA polymerase involved in translesion DNA synthesis, and suppression of REV7 impairs DNA damage tolerance in human fibroblasts (19, 20, 23). During embryogenesis, endogenous factors, such as metabolites, oxygen radicals, and nitrogen species, induce various types of DNA damage, and an effective DNA repair system is very important for normal development of organisms (46–49). Pol ζ is a mispair extender polymerase that extends DNA synthesis from mispaired nucleotides and is necessary for translesion DNA synthesis machinery at various DNA lesions (50). In addition, Pol ζ is involved in homologous recombination repair of the DNA double strand breaks (24, 25). Therefore, it has been suggested that Pol ζ plays a pivotal role in the DNA damage response system. Accordingly, the size of *Rev3*$^{-/-}$ mouse embryos is considerably smaller than that of WT or heterozygote littermates at E9.5–10.5 and abort at around E12.5 (51–54). Extensive apoptosis has been demon-

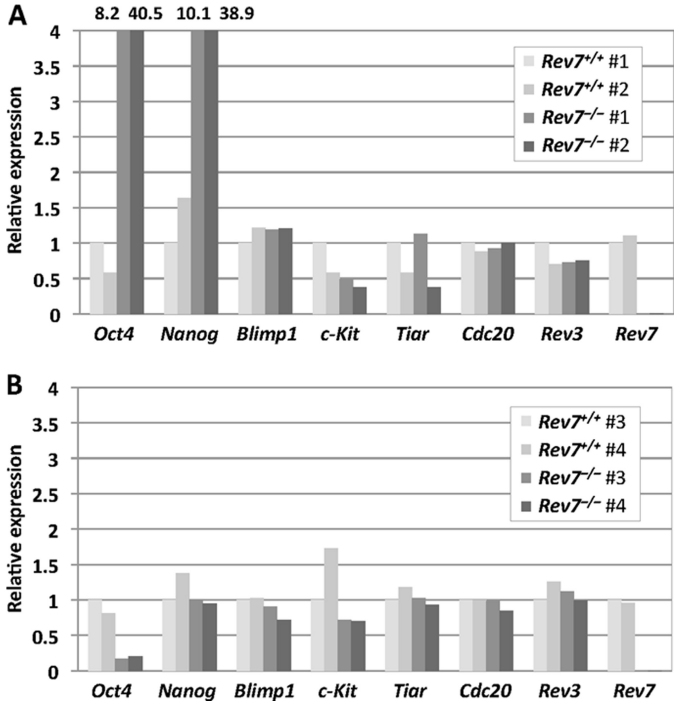

FIGURE 8. **Deregulation of gene expression in *Rev7*$^{-/-}$ embryos.** *A* and *B,* total RNAs were extracted from whole bodies of *Rev7*$^{+/+}$ and *Rev7*$^{-/-}$ embryos at E8.5 (*A*) and from trunks of embryos at E13.5 (*B*). Real-time quantitative RT-PCR was performed using gene-specific primers for *Oct4*, *Nanog*, *Blimp1*, *c-Kit*, *Tiar*, *Cdc20*, *Rev3*, *Rev7,* and *GAPDH* listed in Table 1. The expression levels of each gene in *Rev7*$^{+/+}$ and *Rev7*$^{-/-}$ embryos were determined as relative values to that in *Rev7*$^{+/+}$ #1 (*A*) or *Rev7*$^{+/+}$ #3 (*B*). Relative expression values of *Oct4* and *Nanog* in *Rev7*$^{-/-}$ #1 and #2 embryos are: *Oct4,* 8.2 and 40.5; *Nanog*, 10.1 and 38.9, respectively. Reactions for *GAPDH* are used as internal controls.

strated in all cell lineages of *Rev3*$^{-/-}$ embryos (54). The phenotypes of *Rev7*$^{-/-}$ embryos in this study are similar, in part, to those of *Rev3*$^{-/-}$ embryos, suggesting the possibility that *Rev7*$^{-/-}$ phenotypes are associated with impairment of Pol ζ function. Some experiments using genetically modified mice indicate the importance of the DNA repair system for germ cell maintenance. Disruption of mouse *Rad18*, which is the main regulator of DNA damage tolerance, causes progressive loss of germ cells in the testis after 6 months postnatally, indicating its requirement for long-term maintenance of germ cells (55). Deficient expression of genes involved in nucleotide excision repair, such as *HR23B*, *Ercc1*, and *Xpa*, also impairs normal spermatogenesis and oogenesis in mice (56–58). All of these findings suggest that the DNA repair system is important for germ cells to retain genetic integrity after birth. It is noteworthy that deficiency of REV3 and REV7 causes more severe phenotypes in mouse embryos compared with knock-out phenotypes of other DNA repair genes, suggesting the importance of DNA Pol ζ in mouse embryogenesis.

On the other hand, REV7 is involved in cell cycle regulation by interacting with CDC20 and CDH1 that control the activity of the anaphase-promoting complex to degrade cyclin B1 (27, 28). Homozygous *Cdh1* mutant mice cannot produce normal trophoblasts and die at E9.5–10.5, whereas *Cdc20* knock-out causes metaphase arrest at the two-cell stage and death at a very early embryonic stage (59, 60). Mice lacking the mitotic checkpoint protein MAD2, which is another mammalian homologue of *S. cerevisiae Mad2*, show extensive apoptosis at E7.0 and embryonic lethality during early embryonic stages (61). The *Rev7*$^{-/-}$ phenotypes in the present study were milder than those of *Mad2*$^{-/-}$, *Cdh1*$^{-/-}$, and *Cdc20*$^{-/-}$ mice. The findings that REV7 deficiency caused apoptotic cell death of PGCs and somatic cells, but did not affect cell proliferation, suggest that the *Rev7*$^{-/-}$ phenotypes may not be a consequence of an impairment of cell cycle regulation.

Human REV7 is also involved in gene expression by interacting with transcription factors ELK-1 and TCF-4 (30, 31). REV7 depletion in human cells suppresses up-regulation of the transcriptional activities of ELK-1 after DNA damage, whereas *REV7* knockdown blocks TCF-4-mediated E-cadherin expression and induces N-cadherin and vimentin expression, leading to epithelial-mesenchymal transdifferentiation (30, 31). Mice possessing an Elk-1-null mutation show normal development without any morphological abnormality and only mildly impaired neuronal gene expression (62). *Tcf-4*-null mice die shortly after birth without any gross abnormalities and possess no apparent proliferating cells in the crypt region of the small intestine, suggesting that TCF-4 is necessary for the maintenance of crypt stem cells in the small intestine (63). These mutant mice display phenotypes that are different from those of *Rev7*$^{-/-}$ mice. Interestingly, the phenotype of *Rev7*$^{-/-}$ mice shown in this study is almost the same as that of mice null for the RNA-binding protein TIAR (9). TIAR binds to several mRNAs that encode translation factors and suppresses their translation in response to UV-C irradiation, thereby playing a role as a stress-responsive transcriptional repressor (64). *Tiar*$^{-/-}$ mice show embryonic growth retardation, partial embryonic lethality, reduced numbers of PGCs during migration, and complete ablation of PGCs at E13.5 (9). In human cells, because REV7 is required for damage tolerance and TIAR is needed for stress-response transcriptional repression, it is possible that REV7 is functionally linked to TIAR via gene expression regulation and that the mouse *Rev7*$^{-/-}$ phenotype is associated with the loss-of-function of mouse *Tiar*, although expression of *Tiar* mRNA was unaffected by REV7 deficiency.

In the present study, the significance of REV7 in spermatogenesis after birth could not be analyzed because of germ cell aplasia at birth. Because REV7 is highly expressed in spermatogonia and spermatocytes, suggesting an important role in spermatogenesis after birth, inhibition of REV7 expression by epigenetic alterations after birth might possibly cause impairment of spermatogenesis.

In summary, we established REV7-deficient mice that show growth retardation and progressive loss of PGCs during migration. These results indicate that REV7 is necessary for PGC survival and prevention of apoptotic cell death of somatic cells in the mouse embryo. Further studies are required to elucidate the mechanism of apoptotic cell death that is induced by REV7 deficiency and to clarify the importance of REV7 in human infertility.

Acknowledgments—We thank K. Imaizumi, K. Uchiyama, Y. Hayashi, and A. Ito for technical assistance.

REFERENCES

1. Saga, Y. (2008) Mouse germ cell development during embryogenesis. *Curr. Opin. Genet. Dev.* **18,** 337–341
2. Saitou, M. (2009) Germ cell specification in mice. *Curr. Opin. Genet. Dev.* **19,** 386–395
3. Ewen, K. A., and Koopman, P. (2010) Mouse germ cell development. From specification to sex determination. *Mol. Cell. Endocrinol.* **323,** 76–93
4. Matsui, Y. (2010) Epigenetic profiles in primordial germ cells. Global modulation and fine tuning of the epigenome for acquisition of totipotency. *J. Androl.* **31,** 61–65
5. Ohinata, Y., Payer, B., O'Carroll, D., Ancelin, K., Ono, Y., Sano, M., Barton, S. C., Obukhanych, T., Nussenzweig, M., Tarakhovsky, A., Saitou, M., and Surani, M. A. (2005) Blimp1 is a critical determinant of the germ cell lineage in mice. *Nature* **436,** 207–213
6. Kurimoto, K., Yabuta, Y., Ohinata, Y., Shigeta, M., Yamanaka, K., and Saitou, M. (2008) Complex genome-wide transcription dynamics orchestrated by Blimp1 for the specification of the germ cell lineage in mice. *Genes Dev.* **22,** 1617–1635
7. Yamaji, M., Seki, Y., Kurimoto, K., Yabuta, Y., Yuasa, M., Shigeta, M., Yamanaka, K., Ohinata, Y., and Saitou, M. (2008) Critical function of *Prdm14* for the establishment of the germ cell lineage in mice. *Nat. Genet.* **40,** 1016–1022
8. Tsuda, M., Sasaoka, Y., Kiso, M., Abe, K., Haraguchi, S., Kobayashi, S., and Saga, Y. (2003) Conserved role of nanos proteins in germ cell development. *Science* **301,** 1239–1241
9. Runyan, C., Schaible, K., Molyneaux, K., Wang, Z., Levin, L., and Wylie, C. (2006) Steel factor controls midline cell death of primordial germ cells and is essential for their normal proliferation and migration. *Development* **133,** 4861–4869
10. Beck, A. R., Miller, I. J., Anderson, P., and Streuli, M. (1998) RNA-binding protein TIAR is essential for primordial germ cell development. *Proc. Natl. Acad. Sci. U.S.A.* **95,** 2331–2336
11. Kehler, J., Tolkunova, E., Koschorz, B., Pesce, M., Gentile, L., Boiani, M., Lomelí, H., Nagy, A., McLaughlin, K. J., Schöler, H. R., and Tomilin, A. (2004) Oct4 is required for primordial germ cell survival. *EMBO Rep.* **5,** 1078–1083
12. Youngren, K. K., Coveney, D., Peng, X., Bhattacharya, C., Schmidt, L. S., Nickerson, M. L., Lamb, B. T., Deng, J. M., Behringer, R. R., Capel, B., Rubin, E. M., Nadeau, J. H., and Matin, A. (2005) The *Ter* mutation in the dead end gene causes germ cell loss and testicular germ cell tumours. *Nature* **435,** 360–364
13. Mitsui, K., Tokuzawa, Y., Itoh, H., Segawa, K., Murakami, M., Takahashi, K., Maruyama, M., Maeda, M., and Yamanaka, S. (2003) The homeoprotein Nanog is required for maintenance of pluripotency in mouse epiblast and ES cells. *Cell* **113,** 631–642
14. Seki, Y., Hayashi, K., Itoh, K., Mizugaki, M., Saitou, M., and Matsui, Y. (2005) Extensive and orderly reprogramming of genome-wide chromatin modifications associated with specification and early development of germ cells in mice. *Dev. Biol.* **278,** 440–458
15. Seki, Y., Yamaji, M., Yabuta, Y., Sano, M., Shigeta, M., Matsui, Y., Saga, Y., Tachibana, M., Shinkai, Y., and Saitou, M. (2007) Cellular dynamics associated with the genome-wide epigenetic reprogramming in migrating primordial germ cells in mice. *Development* **134,** 2627–2638
16. Schmahl, J., Eicher, E. M., Washburn, L. L., and Capel, B. (2000) Sry induces cell proliferation in the mouse gonad. *Development* **127,** 65–73
17. Nelson, J. R., Lawrence, C. W., and Hinkle, D. C. (1996) Thymine-thymine dimer bypass by yeast DNA polymerase ζ. *Science* **272,** 1646–1649
18. Guo, C., Kosarek-Stancel, J. N., Tang, T. S., and Friedberg, E. C. (2009) Y-family DNA polymerases in mammalian cells. *Cell. Mol. Life Sci.* **66,** 2363–2381
19. Murakumo, Y., Roth, T., Ishii, H., Rasio, D., Numata, S., Croce, C. M., and Fishel, R. (2000) A human REV7 homolog that interacts with the polymerase ζ catalytic subunit hREV3 and the spindle assembly checkpoint protein hMAD2. *J. Biol. Chem.* **275,** 4391–4397
20. Murakumo, Y., Ogura, Y., Ishii, H., Numata, S., Ichihara, M., Croce, C. M., Fishel, R., and Takahashi, M. (2001) Interactions in the error-prone postreplication repair proteins hREV1, hREV3, and hREV7. *J. Biol. Chem.* **276,** 35644–35651
21. Masuda, Y., Ohmae, M., Masuda, K., and Kamiya, K. (2003) Structure and enzymatic properties of a stable complex of the human REV1 and REV7 proteins. *J. Biol. Chem.* **278,** 12356–12360
22. Hara, K., Hashimoto, H., Murakumo, Y., Kobayashi, S., Kogame, T., Unzai, S., Akashi, S., Takeda, S., Shimizu, T., and Sato, M. (2010) Crystal structure of human REV7 in complex with a human REV3 fragment and structural implication of the interaction between DNA polymerase ζ and REV1. *J. Biol. Chem.* **285,** 12299–12307
23. McNally, K., Neal, J. A., McManus, T. P., McCormick, J. J., and Maher, V. M. (2008) hRev7, putative subunit of hPolζ, plays a critical role in survival, induction of mutations, and progression through S-phase, of UV_{254nm}-irradiated human fibroblasts. *DNA Repair* **7,** 597–604
24. Okada, T., Sonoda, E., Yoshimura, M., Kawano, Y., Saya, H., Kohzaki, M., and Takeda, S. (2005) Multiple roles of vertebrate *REV* genes in DNA repair and recombination. *Mol. Cell. Biol.* **25,** 6103–6111
25. Sharma, S., Hicks, J. K., Chute, C. L., Brennan, J. R., Ahn, J. Y., Glover, T. W., and Canman, C. E. (2012) REV1 and polymerase ζ facilitate homologous recombination repair. *Nucleic Acids Res.* **40,** 682–691
26. Cahill, D. P., da Costa, L. T., Carson-Walter, E. B., Kinzler, K. W., Vogelstein, B., and Lengauer, C. (1999) Characterization of *MAD2B* and other mitotic spindle checkpoint genes. *Genomics* **58,** 181–187
27. Chen, J., and Fang, G. (2001) MAD2B is an inhibitor of the anaphase-promoting complex. *Genes Dev.* **15,** 1765–1770
28. Pfleger, C. M., Salic, A., Lee, E., and Kirschner, M. W. (2001) Inhibition of Cdh1-APC by the MAD2-related protein MAD2L2. A novel mechanism for regulating Cdh1. *Genes Dev.* **15,** 1759–1764
29. Iwai, H., Kim, M., Yoshikawa, Y., Ashida, H., Ogawa, M., Fujita, Y., Muller, D., Kirikae, T., Jackson, P. K., Kotani, S., and Sasakawa, C. (2007) A bacterial effector targets Mad2L2, an APC inhibitor, to modulate host cell cycling. *Cell* **130,** 611–623
30. Zhang, L., Yang, S. H., and Sharrocks, A. D. (2007) Rev7/MAD2B links c-Jun N-terminal protein kinase pathway signaling to activation of the transcription factor Elk-1. *Mol. Cell. Biol.* **27,** 2861–2869
31. Hong, C. F., Chou, Y. T., Lin, Y. S., and Wu, C. W. (2009) MAD2B, a novel TCF4-binding protein, modulates TCF4-mediated epithelial-mesenchymal transdifferentiation. *J. Biol. Chem.* **284,** 19613–19622
32. Weterman, M. A., van Groningen, J. J., Tertoolen, L., and van Kessel, A. G. (2001) Impairment of MAD2B-PRCC interaction in mitotic checkpoint defective t(X;1)-positive renal cell carcinomas. *Proc. Natl. Acad. Sci. U.S.A.* **98,** 13808–13813
33. Li, L., Shi, Y., Wu, H., Wan, B., Li, P., Zhou, L., Shi, H., and Huo, K. (2007) Hepatocellular carcinoma-associated gene 2 interacts with MAD2L2. *Mol. Cell. Biochem.* **304,** 297–304
34. Rimkus, C., Friederichs, J., Rosenberg, R., Holzmann, B., Siewert, J. R., and Janssen, K. P. (2007) Expression of the mitotic checkpoint gene *MAD2L2* has prognostic significance in colon cancer. *Int. J. Cancer* **120,** 207–211
35. Matsunami, H., and Takeichi, M. (1995) Fetal brain subdivisions defined by R- and E-cadherin expressions: evidence for the role of cadherin activity in region-specific, cell-cell adhesion. *Dev. Biol.* **172,** 466–478
36. Chen, T., Du, J., and Lu, G. (2012) Cell growth arrest and apoptosis induced by Oct4 or Nanog knockdown in mouse embryonic stem cells. A possible role of Trp53. *Mol. Biol. Rep.* **39,** 1855–1861
37. Anderson, R., Fässler, R., Georges-Labouesse, E., Hynes, R. O., Bader, B. L., Kreidberg, J. A., Schaible, K., Heasman, J., and Wylie, C. (1999) Mouse primordial germ cells lacking β1 integrins enter the germline but fail to migrate normally to the gonads. *Development* **126,** 1655–1664
38. Wilkinson, D. G., and Nieto, M. A. (1993) Detection of messenger RNA by *in situ* hybridization to tissue sections and whole mounts. *Methods Enzymol.* **225,** 361–373
39. Matzuk, M. M., and Lamb, D. J. (2002) Genetic dissection of mammalian fertility pathways. *Nat. Cell Biol.* **4,** s41–49
40. Ombelet, W., Cooke, I., Dyer, S., Serour, G., and Devroey, P. (2008) Infertility and the provision of infertility medical services in developing countries. *Hum. Reprod. Update* **14,** 605–621
41. Ferlin, A., Arredi, B., and Foresta, C. (2006) Genetic causes of male infertility. *Reprod. Toxicol.* **22,** 133–141
42. Saitou, M., and Yamaji, M. (2010) Germ cell specification in mice. Signal-

ing, transcription regulation, and epigenetic consequences. *Reproduction* **139,** 931–942
43. Schöler, H. R., Dressler, G. R., Balling, R., Rohdewohld, H., and Gruss, P. (1990) Oct-4, a germline-specific transcription factor mapping to the mouse t-complex. *EMBO J.* **9,** 2185–2195
44. Yeom, Y. I., Fuhrmann, G., Ovitt, C. E., Brehm, A., Ohbo, K., Gross, M., Hübner, K., and Schöler, H. R. (1996) Germline regulatory element of Oct-4 specific for the totipotent cycle of embryonal cells. *Development* **122,** 881–894
45. Chambers, I., Colby, D., Robertson, M., Nichols, J., Lee, S., Tweedie, S., and Smith, A. (2003) Functional expression cloning of Nanog, a pluripotency sustaining factor in embryonic stem cells. *Cell* **113,** 643–655
46. Burcham, P. C. (1999) Internal hazards. Baseline DNA damage by endogenous products of normal metabolism. *Mutat. Res.* **443,** 11–36
47. Wink, D. A., Kasprzak, K. S., Maragos, C. M., Elespuru, R. K., Misra, M., Dunams, T. M., Cebula, T. A., Koch, W. H., Andrews, A. W., and Allen, J. S. (1991) DNA deaminating ability and genotoxicity of nitric oxide and its progenitors. *Science* **254,** 1001–1003
48. Jaroudi, S., and SenGupta, S. (2007) DNA repair in mammalian embryos. *Mutat. Res.* **635,** 53–77
49. Vinson, R. K., and Hales, B. F. (2002) DNA repair during organogenesis. *Mutat. Res.* **509,** 79–91
50. Waters, L. S., Minesinger, B. K., Wiltrout, M. E., D'Souza, S., Woodruff, R. V., and Walker, G. C. (2009) Eukaryotic translesion polymerases and their roles and regulation in DNA damage tolerance. *Microbiol. Mol. Biol. Rev.* **73,** 134–154
51. Bemark, M., Khamlichi, A. A., Davies, S. L., and Neuberger, M. S. (2000) Disruption of mouse polymerase ζ (Rev3) leads to embryonic lethality and impairs blastocyst development *in vitro*. *Curr. Biol.* **10,** 1213–1216
52. Wittschieben, J., Shivji, M. K., Lalani, E., Jacobs, M. A., Marini, F., Gearhart, P. J., Rosewell, I., Stamp, G., and Wood, R. D. (2000) Disruption of the developmentally regulated *Rev3l* gene causes embryonic lethality. *Curr. Biol.* **10,** 1217–1220
53. Esposito, G., Godindagger, I., Klein, U., Yaspo, M. L., Cumano, A., and Rajewsky, K. (2000) Disruption of the *Rev3l*-encoded catalytic subunit of polymerase ζ in mice results in early embryonic lethality. *Curr. Biol.* **10,** 1221–1224
54. Van Sloun, P. P., Varlet, I., Sonneveld, E., Boei, J. J., Romeijn, R. J., Eeken, J. C., and De Wind N. (2002) Involvement of mouse *Rev3* in tolerance of endogenous and exogenous DNA damage. *Mol. Cell. Biol.* **22,** 2159–2169
55. Sun, J., Yomogida, K., Sakao, S., Yamamoto, H., Yoshida, K., Watanabe, K., Morita, T., Araki, K., Yamamura, K., and Tateishi, S. (2009) Rad18 is required for long-term maintenance of spermatogenesis in mouse testes. *Mech. Dev.* **126,** 173–183
56. Ng, J. M., Vrieling, H., Sugasawa, K., Ooms, M. P., Grootegoed, J. A., Vreeburg, J. T., Visser, P., Beems, R. B., Gorgels, T. G., Hanaoka, F., Hoeijmakers, J. H., and van der Horst, G. T. (2002) Developmental defects and male sterility in mice lacking the ubiquitin-like DNA repair gene *mHR23B*. *Mol. Cell. Biol.* **22,** 1233–1245
57. Hsia, K. T., Millar, M. R., King, S., Selfridge, J., Redhead, N. J., Melton, D. W., and Saunders, P. T. (2003) DNA repair gene *Ercc1* is essential for normal spermatogenesis and oogenesis and for functional integrity of germ cell DNA in the mouse. *Development* **130,** 369–378
58. Nakane, H., Hirota, S., Brooks, P. J., Nakabeppu, Y., Nakatsu, Y., Nishimune, Y., Iino, A., and Tanaka, K. (2008) Impaired spermatogenesis and elevated spontaneous tumorigenesis in xeroderma pigmentosum group A gene (*Xpa*)-deficient mice. *DNA Repair* **7,** 1938–1950
59. Li, M., York, J. P., and Zhang, P. (2007) Loss of Cdc20 causes a securin-dependent metaphase arrest in two-cell mouse embryos. *Mol. Cell. Biol.* **27,** 3481–3488
60. García-Higuera, I., Manchado, E., Dubus, P., Cañamero, M., Méndez, J., Moreno, S., and Malumbres, M. (2008) Genomic stability and tumour suppression by the APC/C cofactor Cdh1. *Nat. Cell. Biol.* **10,** 802–811
61. Dobles, M., Liberal, V., Scott, M. L., Benezra, R., and Sorger, P. K. (2000) Chromosome missegregation and apoptosis in mice lacking the mitotic checkpoint protein Mad2. *Cell* **101,** 635–645
62. Cesari, F., Brecht, S., Vintersten, K., Vuong, L.G., Hofmann, M., Klingel, K., Schnorr, J. J., Arsenian, S., Schild, H., Herdegen, T., Wiebel, F. F., and Nordheim, A. (2004) Mice deficient for the Ets transcription factor Elk-1 show normal immune responses and mildly impaired neuronal gene activation. *Mol. Cell. Biol.* **24,** 294–305
63. Korinek, V., Barker, N., Moerer, P., van Donselaar, E., Huls, G., Peters, P. J., and Clevers H. (1998) Depletion of epithelial stem-cell compartments in the small intestine of mice lacking Tcf-4. *Nat. Genet.* **19,** 379–383
64. Mazan-Mamczarz, K., Lal, A., Martindale, J. L., Kawai, T., and Gorospe, M. (2006) Translational repression by RNA-binding protein TIAR. *Mol. Cell. Biol.* **26,** 2716–2727